Electronics **2015**, *4*, 723-738; doi:10.3390/electronics4040723

OPEN ACCESS

electronics

ISSN 2079-9292

www.mdpi.com/journal/electronics

Article

Theoretical Analysis of Vibration Frequency of Graphene Sheets Used as Nanomechanical Mass Sensor

Toshiaki Natsuki [1,2]

[1] Faculty of Textile Science and Technology, Shinshu University, 3-15-1 Tokida, Ueda-shi 386-8567, Japan; E-Mail: natsuki@shinshu-u.ac.jp; Tel.: +81-268-21-5421

[2] Institute of Carbon Science and Technology, Shinshu University, 4-17-1 Wakasato, Nagano 380-8553, Japan

Academic Editor: Frank Schwierz

Received: 8 April 2015 / Accepted: 21 August 2015 / Published: 28 September 2015

Abstract: Nanoelectromechanical resonator sensors based on graphene sheets (GS) show ultrahigh sensitivity to vibration. However, many factors such as the layer number and dimension of the GSs will affect the sensor characteristics. In this study, an analytical model is proposed to investigate the vibration behavior of double-layered graphene sheets (DLGSs) with attached nanoparticles. Based on nonlocal continuum mechanics, the influences of the layer number, dimensions of the GSs, and of the mass and position of nanoparticles attached to the GSs on the vibration response of GS resonators are discussed in detail. The results indicate that nanomasses can easily be detected by GS resonators, which can be used as a highly sensitive nanomechanical element in sensor systems. A logarithmically linear relationship exists between the frequency shift and the attached mass when the total mass attached to GS is less than about 1.0 zg. Accordingly, it is convenient to use a linear calibration for the calculation and determination of attached nanomasses. The simulation approach and the parametric investigation are useful tools for the design of graphene-based nanomass sensors and devices.

Keywords: graphene sheet; nonlocal elasticity theory; vibration; nanosensor

1. Introduction

Graphene sheets (GSs) have attracted great attention due to their extraordinary mechanical, electrical and thermal properties [1–3]. These fascinating carbon nanomaterials have many potential applications, such as reinforced materials, solar cells, molecule sensors and nanomechanical resonators [4–9]. Jang and his group [10–12] performed molecular dynamics (MD) simulation to investigate the mass sensitivity and resonant frequency of graphene nanomechanical resonators (GNMRs), the temperature-dependent scaling transition in the quality factors of GNMRs, and the effect of polar surfaces on the quality (Q)-factors of zinc oxide (ZnO) nanoresonators. The basic principle of nanoresonator sensors is the detection of a shift of the resonant frequency or wave velocity in the nanosensors caused by attached nanoparticles, including atoms or molecules. The sensitivity of the sensors and their applicability in distinguishing distinct types of atoms/molecules have been discussed by Wand and Arash [13], who simulated the detection of gas atoms based on wave velocity shifts in single-walled carbon nanotubes (SWCNTs) and explored the efficiency of nanotube-based sensors [14].

For structural applications of GSs, knowing their macroscopic properties is required. Therefore, both experimental and theoretical studies of GSs are important issues to design optimal materials and devices. At present, GSs are extensively investigated for applications in optoelectronic devices, high-performance hybrid supercapacitors, and various types of high performance sensors. Nanoelectromechanical systems (NEMS) are emerging as strong candidates for a host of important applications in semiconductor-based technology and fundamental science [15]. Graphene-based NEMS resonators could provide higher sensitivity as nanomechanical mass sensor. The operation of a NEMS mass sensor relies on monitoring how the resonance frequency of a nanomechanical resonator changes when an additional nanomass is adsorbed on its surface [16–18]. There is a fast-growing interest in GSs for use in NEMS resonators, given that lightness and stiffness are the essential characteristics sought after in NEMS resonators for sensing applications [19]. NEMS resonators can be fabricated based on single-layered (SLGSs) or multi-layered graphene sheets (MLGSs) by mechanically exfoliating thin sheets from graphite and putting them over trenches in a silicon oxide layer. Vibrations with fundamental resonant frequency in the megahertz range were actuated, either optically or electrically, and detected optically by interferometry [20].

Current efforts in graphene synthesis include micromechanical cleavage, liquid-phase exfoliation, chemical vapor deposition (CVD), and carbon segregation [21–25]. Double-layered graphene sheets (DLGSs) consist of two single GSs coupled by van der Waals (vdW) interaction forces, and can be synthesized on a silicon carbide substrate [26–28]. DLGSs are of considerable interest because of their unique electronic bands and mechanical properties. Different from SLGSs, the bandgap of DLGSs can be controlled externally by a gate bias and gaps up to 250 meV can be opened, which reveals the large potential of DLGSs for applications in NEMS [29–32]. On the other hand, DLGSs have higher stiffness and natural frequency than SLGSs because of the vdW interaction forces [33–35]. Thus, the resonance frequency and the frequency shift of DLGSs used as NEMS mass sensors can be measured more obviously.

NEMS mass sensors with a resonator can be fabricated from GSs, and the sensing mechanism is based on the fact that the resonant frequency is sensitive to changes in the attached mass [36]. Recently, various theoretical studies have been carried out utilizing the molecular dynamics (MD) method [37,38],

molecular structural mechanics [39], or continuum mechanics [35,40–43] to investigate SLGSs for use in NEMS mass sensors. Arash *et al.* studied the vibration properties of SLGSs with five noble gas atoms (He, Ne, Ar, Kr, and Xe) attached using MD simulation to evaluate the applicability of graphene mass sensors [37]. The results indicate that the resolution of a mass sensor made of a square-shaped graphene sheet with a size of 10 nm could achieve an order of 10^{-24} kg and the mass sensitivity could be enhanced by decreasing the size of the SLGSs. Sakhaee-Pour *et al.* investigated the vibration behavior of defect-free SLGSs using molecular structural mechanics [39]. The principal frequency was highly sensitive to an added nanomass of the order of 10^{-24} kg, corresponding to Reference [37]. Based on a continuum elastic model, Lei *et al.* [39] analyzed the sensitivity of frequency shift of an atomic-resolution nanomechanical mass sensor modeled by a circular SLGS with attached nanoparticles. The sensitivity of such mass sensor could reach 10^{-27} kg. The effects of the nonlocal parameters and the attached mass on the frequency shifts of GSs were investigated using a nonlocal continuum elastic model [42,43]. The obtained results show that the frequency shift of the SLGS became smaller when the effect of nonlocal parameters was taken into account. Shen *et al.* [42] did the comparison between the continuum mechanics and the finite element method (FEM) and found a good agreement. This means that the SLGSs with an attached nanoparticle can be simulated accurately based on continuum mechanics. At present, the studies of the mass detection using the graphene-based nanomechanical sensor are focused solely on SLGSs. Because the resonance frequency and its frequency shift of DLGSs resonant could be measured more obviously, DLGSs based mass sensors need to be studied [44].

Ultrasonic vibration and attenuation are important properties related to the design and performance of the sensor devices. GSs appear to be excellent element materials for nanomechanical resonators because they can generate vibrations in the terahertz range. So far, only little has been reported on the resonant frequency analysis for DLGSs used as nanomass sensor, and it is the purpose of the present study to remedy this deficiency. We explore the potential of DLGSs used as a NEMS mass sensor, considering that DLGSs have higher strength and vibration frequency than SLGSs. Based on a nonlocal continuum theory, the influences of the mass and position of attached nanoparticles, of the dimensions of DLGSs, and of nonlocal parameters on the vibration response of DLGS sensor are investigated in detail.

2. Experimental Approach

2.1. Nonlocal Elasticity Theory

According to the general elasticity model, the stress components at any point depend only on the strain component at the same point. In the nonlocal elasticity theory, the stress field at a certain point is considered to be a function of the strain distribution over a certain representative volume of the material centered at that point. The nonlocal elasticity theory [45–47] can be used to study several phenomena related to nanoscale materials. For nonlocal linear elastic solids, the constitutive equation of motion is given by

$$\boldsymbol{t}_{ij,j} + \boldsymbol{f}_i = \rho \ddot{\boldsymbol{u}}_i \tag{1}$$

where $\boldsymbol{\rho}$ and $\boldsymbol{f_i}$ are the mass density and the applied body forces, respectively, $\boldsymbol{u_i}$ is the displacement vector, and $\boldsymbol{t_{ij}}$ is the stress tensor of the nonlocal elasticity expressed as

$$\boldsymbol{t}_{ij} = \int_V \alpha\left(|\boldsymbol{x}-\boldsymbol{x}'|, e_0 a\right)\boldsymbol{\sigma}_{ij}(\boldsymbol{x}')dV(\boldsymbol{x}') \tag{2}$$

where $\boldsymbol{x}$ is a reference point in the body, e_0 is a constant appropriate to the material and has to be determined for each materials independently by experiments or atomistic simulation, a is the internal characteristic length (e.g., lattice parameter, granular size, distance between atoms bound), $|x - x'|$ is the Euclidean distance, and V is an integral region occupied by the body. The nonlocal kernel function $\alpha(|x - x'|, e_0 a)$ incorporates the nonlocal effects into the constitutive equation and is given as

$$\alpha\left(|\boldsymbol{x}-\boldsymbol{x}'|, e_0 a\right) = \frac{1}{2\pi(e_0 a)^2} K_0\left(\frac{\sqrt{\boldsymbol{x}\cdot\boldsymbol{x}}}{e_0 a}\right) \tag{3}$$

where K_0 is the modified Bessel function.

In Equation (2), $\boldsymbol{\sigma_{ij}}$ is the local stress tensor of the classical elasticity theory at any point $\boldsymbol{x}'$ in the body and satisfies the constitutive relations

$$\boldsymbol{\sigma_{ij}}(\boldsymbol{x}') = \lambda\boldsymbol{\varepsilon_{kk}}(\boldsymbol{x}')\delta_{ij} + 2\mu\boldsymbol{\varepsilon_{ij}}(\boldsymbol{x}') \tag{4}$$

where λ and μ are the Lame constants and $\boldsymbol{\varepsilon_{ij}}$ is the strain tensor.

For two-dimensional nonlocal elastic beam theory, the stress–strain relation can be expressed as

$$\boldsymbol{\sigma_{ij}} - (e_0 a)^2\nabla^2\boldsymbol{\sigma_{ij}} = \lambda\boldsymbol{\varepsilon_{kk}}(\boldsymbol{x}')\delta_{ij} + 2\mu\boldsymbol{\varepsilon_{ij}}(\boldsymbol{x}') \tag{5}$$

where ∇ is the Laplace operator, which is given as $\partial^2/\partial x_1^2 + \partial^2/\partial x_2^2$ in a two-dimensional rectangular coordinate system (x_1, x_2).

The nonlocal elasticity model has been widely adopted for tackling various problems of linear elasticity and micro- or nanostructural mechanics.

2.2. Single-Layer Graphene Sheets

Based on nonlocal continuum mechanics, we consider the dynamic behavior of a single-layer graphene sheet (SLGS) with an attached concentrated mass m_c located at an arbitrary position (x_0, y_0) as shown in Figure 1. The origin is taken at one corner of the mid-plane of the graphene sheet. The x- and y-axes are taken along the length L_a and width L_b of the SLGS, respectively, and the z-axis is taken along the thickness h of the SLGS.

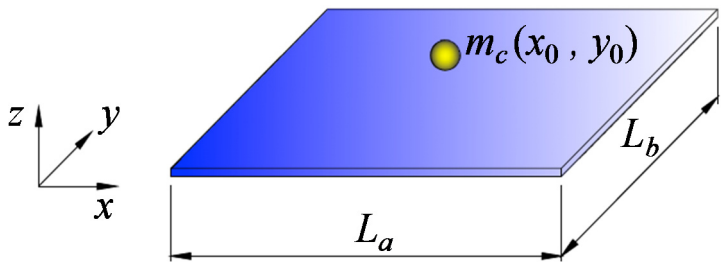

Figure 1. Schematic illustration showing a single-walled GS with an attached mass.

Using the nonlocal elasticity theory, the two-dimensional nonlocal constitutive equations of SLGS are given as

$$\sigma_{xx} - (e_0 a)^2 \left(\frac{\sigma_{xx}^2}{\partial x^2} + \frac{\sigma_{xx}^2}{\partial y^2} \right) = \frac{E}{1-\nu^2} \left(\varepsilon_{xx} + \nu \varepsilon_{yy} \right) \tag{6a}$$

$$\sigma_{yy} - (e_0 a)^2 \left(\frac{\sigma_{yy}^2}{\partial x^2} + \frac{\sigma_{yy}^2}{\partial y^2} \right) = \frac{E}{1-\nu^2} \left(\varepsilon_{yy} + \nu \varepsilon_{xx} \right) \tag{6b}$$

$$\tau_{xy} - (e_0 a)^2 \left(\frac{\sigma_{xy}^2}{\partial x^2} + \frac{\sigma_{xy}^2}{\partial y^2} \right) = G \gamma_{xy} \tag{6c}$$

where E, G and v are the elastic modulus, the shear modulus, and Poisson's ratio of the GSs, respectively. The internal characteristic length a is the distance between two atoms in a C-C bond, which is 0.142 nm.

The flexural moments of SLGS are obtained from

$$M_{xx} = \int_{-h/2}^{h/2} z \sigma_{xx} dz \tag{7a}$$

$$M_{yy} = \int_{-h/2}^{h/2} z \sigma_{yy} dz \tag{7b}$$

$$M_{xy} = \int_{-h/2}^{h/2} z \tau_{xy} dz \tag{7c}$$

When neglecting the displacements of the middle surface in the x and y directions, the relationship between strain and displacement fields is expressed as

$$\varepsilon_{xx} = -z \frac{\partial^2 w}{\partial x^2} \tag{8a}$$

$$\varepsilon_{yy} = -z \frac{\partial^2 w}{\partial y^2} \tag{8b}$$

$$\gamma_{xx} = -2z \frac{\partial^2 w}{\partial x \partial y} \tag{8c}$$

where w is the displacement along the thickness of GSs.

Substituting Equation (6) into Equation (7) and using Equation (8), we have

$$M_{xx} - (e_0 a)^2 \left(\frac{\partial^2 M_{xx}}{\partial x^2} + \frac{\partial^2 M_{xx}}{\partial y^2} \right) = -D \left(\frac{\partial^2 w}{\partial x^2} + \nu \frac{\partial^2 w}{\partial y^2} \right) \tag{9a}$$

$$M_{yy} - (e_0 a)^2 \left(\frac{\partial^2 M_{yy}}{\partial x^2} + \frac{\partial^2 M_{yy}}{\partial y^2} \right) = -D \left(\frac{\partial^2 w}{\partial y^2} + \nu \frac{\partial^2 w}{\partial x^2} \right) \tag{9b}$$

$$M_{xy} - (e_0 a)^2 \left(\frac{\partial^2 M_{xy}}{\partial x^2} + \frac{\partial^2 M_{xy}}{\partial y^2} \right) = -D(1-\nu) \frac{\partial^2 w}{\partial x \partial y} \tag{9c}$$

where D is the flexural rigidity of SLGS, expressed as

$$D = \frac{Eh^3}{12(1-\nu^2)} \tag{9d}$$

The governing equation for the flexural vibration of SLGS carrying a nanoparticle can be given as

$$\frac{\partial^2 M_{xx}}{\partial x^2} + 2\frac{\partial^2 M_{xy}}{\partial x \partial y} + \frac{\partial^2 M_{yy}}{\partial y^2} = [\rho h + m_c \delta(x - x_0)\delta(y - y_0)]\frac{\partial^2 w}{\partial t^2} \tag{10}$$

where ρ is the mass density of SLGS, m_c is the mass of nanoparticles attached at the position (x_0, y_0), and δ is the Dirac delta function denoted as

$$\delta(x) = \begin{cases} +\infty, & x = 0 \\ 0, & x \neq 0 \end{cases} \tag{11}$$

Substituting Equation (9) into Equation (10), the governing equation can be written in terms of w as

$$D\left(\frac{\partial^4 w}{\partial x^4} + 2\frac{\partial^4 w}{\partial x^2 \partial y^2} + \frac{\partial^4 w}{\partial y^4}\right) + \left[1 - (e_0 a)^2\left(\frac{\partial^2 w}{\partial x^2} + \frac{\partial^2 w}{\partial y^2}\right)\right][\rho h + m_c \delta(x - \xi)\delta(x - \eta)]\frac{\partial^2 w}{\partial t^2} = 0 \tag{12}$$

The harmonic solution of Equation (12) can be expressed as

$$w(x, y, t) = Y(x, y)\, e^{i\omega t} \tag{13}$$

where $Y(x,y)$ is the shape function of deflection and ω is the resonant frequency of the SLGS.

Substituting Equation (13) into Equation (12), we obtain

$$\left(\frac{\partial^4 Y}{\partial x^4} + 2\frac{\partial^4 Y}{\partial x^2 \partial y^2} + \frac{\partial^4 Y}{\partial y^4}\right) - \frac{\omega^2}{D}\left[1 - (e_0 a)^2\left(\frac{\partial^2 Y}{\partial x^2} + \frac{\partial^2 Y}{\partial y^2}\right)\right][\rho h + m_c \delta(x - \xi)\delta(x - \eta)]\frac{\partial^2 Y}{\partial x^2} = 0 \tag{14}$$

Note that the boundary conditions of SLGS with simply supported edges are

$$w = 0, \quad \frac{\partial^2 w}{\partial x^2} = 0, \quad \frac{\partial^2 w}{\partial y^2} = 0 \text{ on } x = 0, L_a \text{ and } y = 0, L_b \tag{15}$$

Therefore, the shape function (Y) in Equation (13) can be expressed as

$$Y(x, y) = A_{mn} \sin\frac{m\pi x}{L_a} \sin\frac{n\pi y}{L_b} \tag{16}$$

where A_{mn} is the vibration amplitude of oscillation and m and n indicate the mode numbers in the periodic directions.

Substituting the shape function of Equation (16) into Equation (14), then multiplying both sides of Equation (14) by $\sin\frac{m\pi x}{L_a}\sin\frac{n\pi y}{L_b}$ and integrating over the whole region with respect to x and y with the limits $x = 0$ to $x = L_a$ and $y = 0$ to $y = L_b$, after some simplifications, we obtain the following frequency equation

$$\begin{aligned} &\int_0^b \int_0^a A_{mn} D\pi^4 \left(\frac{m^2}{L_a^2} + \frac{n^2}{L_b^2}\right)^2 \sin^2\frac{m\pi x}{L_a} \sin^2\frac{n\pi y}{L_b}\, dxdy \\ &- \omega^2 \int_0^b \int_0^a A_{mn}\left[1 + (e_0 a)^2 \pi^2\left(\frac{m^2}{L_a^2} + \frac{n^2}{L_b^2}\right)\right][\rho h + m_c \delta(x - \xi)\delta(x - \eta)]\sin^2\frac{m\pi x}{L_a} \sin^2\frac{n\pi y}{L_b}\, dxdy = 0 \end{aligned} \tag{17}$$

All roots of the above equation are the desired resonant frequencies corresponding to a given shape function. The coefficient of A_{mn} should be zero for the non-trivial solution. Thus, the resonant frequency of mass sensor can be determined from

$$\omega_{mn}^2 = \frac{D\pi^4\left(\frac{m^2}{L_a^2}+\frac{n^2}{L_b^2}\right)^2}{\left[1+(e_0a)^2\pi^2\left(\frac{m^2}{L_a^2}+\frac{n^2}{L_b^2}\right)\right]\left(\rho h+\frac{4m_c}{L_aL_b}\sin^2 m\pi\xi\sin^2 n\pi\eta\right)} \tag{18}$$

When the nonlocal parameter (e_0a) is assumed to be zero, the resonant frequency of a SLGS with attached nanoparticles can also be obtained from classical elasticity theory.

2.3. Double-Layer Graphene Sheets

DLGSs are composed of two single layers of GSs, interacting with each other by vdW forces. To the upper sheet of DLGSs nanoparticles are attached while no nanoparticles are attached to the lower graphene sheet. Thus, the governing equations for the vibration of the DLGS are given as the two coupled equations

$$D\nabla^4 w_1 + \left[1-(e_0a)^2\nabla^2\right]\left[\rho h + m_c\delta(x-x_0)\delta(y-y_0)\right]\frac{\partial^2 w_1}{\partial t^2} = p_{12} \tag{19a}$$

$$D\nabla^4 w_2 + \rho h\left[1-(e_0a)^2\nabla^2\right]\frac{\partial^2 w_2}{\partial t^2} = p_{21} \tag{19b}$$

where $w_j(x,y,t), j = 1,2$, are the flexural deflections of the upper ($j = 1$) and lower ($j = 2$) sheet, p_{12} ($p_{21} = -p_{12}$) is the transverse pressure caused by the vdW forces between the two layers of DLGSs, ρ is the mass density of the GSs, h is the thickness of each layer in DLGSs, t is the time, and δ is the Dirac delta function. The bi-harmonic operator and the flexural rigidity are given by

$$\nabla^4 = \frac{\partial^4}{\partial x^4}+\frac{\partial^4}{\partial x^2\partial y^2}+\frac{\partial^4}{\partial y^4},\ D = \frac{Eh^3}{12\left(1-\nu^2\right)} \tag{20}$$

where E is the elastic modulus of GSs and v is Poisson' s ratio.

In Equation (19), the distributed transverse pressure acting on the upper and lower layers of DLGSs can be given by

$$p_{12} = c\left(w_2 - w_1\right) \tag{21}$$

where c is the vdW interaction coefficient between the upper and lower layers, which can be obtained from the Lennard–Jones pair potential [48], given as:

$$c = b\left(\frac{4\sqrt{3}}{9a}\right)^2\frac{24\varepsilon}{\sigma^2}\left(\frac{\sigma}{a}\right)^8\left[\frac{3003\pi}{256}\sum_{k=0}^{5}\frac{(-1)^k}{2k+1}\binom{5}{k}\left(\frac{\sigma}{a}\right)^6\frac{1}{\left(\bar{z}_1-\bar{z}_2\right)^{12}} - \frac{35\pi}{8}\sum_{k=0}^{2}\frac{(-1)^k}{2k+1}\frac{1}{\left(\bar{z}_1-\bar{z}_2\right)^6}\right] \tag{22}$$

Here, $\varepsilon = 2.968\ meV$ and $\sigma = 0.34\ nm$ are parameters determined by the physical properties of GSs, $\bar{z}_j = z_j/a$, $(j = 1, 2)$, where z_j is the coordinate of the *j*th layer in the direction of thickness with the origin at the midplane of the GSs, and $a = 1.42\ nm$ is the C-C bond length.

In Equation (19), we define the following function:

$$\mu(x, y) = \rho h + m_c \delta(x - x_0)\delta(y - y_0) \tag{23}$$

Thus, μ is the variable mass distribution function of the upper sheet.

To obtain the vibration frequency for the governing equations Equation (19) of DLGS, we can introduce the substitution

$$w_j(x, y, t) = Y_j(x, y)\, e^{i\omega t}, \quad j = 1, 2 \tag{24}$$

where $Y_j\ (x, y), j = 1, 2$ is the shape function of deflection in the upper and lower sheets and ω is the resonant frequency of the DLGS sensor.

Substituting Equation (24) into Equation (19), the coupled governing equations of the vibration in DLGSs are written in following matrix form:

$$\begin{bmatrix} D\nabla^4 + \mu\omega^2 (e_0 a)^2 \nabla^2 + c - \mu\omega^2 & -c \\ -c & D\nabla^4 + \rho h\omega^2 (e_0 a)^2 \nabla^2 + c - \rho h\omega^2 \end{bmatrix} \begin{Bmatrix} Y_1 \\ Y_2 \end{Bmatrix} = \begin{Bmatrix} 0 \\ 0 \end{Bmatrix} \tag{25}$$

Algebraic manipulation of Equation (25) reduces it to a single equation:

$$\begin{aligned} &\nabla^8 Y + \frac{(\mu + \rho h)\omega^2 (e_0 a)^2}{D} \nabla^6 Y + \frac{\left(2c - \rho h\omega^2 - \mu\omega^2\right) D + \mu\rho h\omega^4 (e_0 a)^4}{D^2} \nabla^4 Y \\ &+ \frac{\left[c(\rho h + \mu) - 2\rho h\omega^2\right]\omega^2 (e_0 a)^2}{D^2} \nabla^2 Y + \left[\frac{\rho h\mu\omega^4 - c(\rho h + \mu)\omega^2}{D^2}\right] Y = 0 \end{aligned} \tag{26}$$

where $Y = Y_1$, or $Y = Y_2$.

For a simply supported boundary condition, the shape function of deflection of DLGS in Equation (26) can be expressed as

$$Y(x, y) = C_{mn} \sin\frac{m\pi x}{L_a} \sin\frac{n\pi y}{L_b} \tag{27}$$

where C_{mn} is the vibration amplitude of oscillation and *m* and *n* indicate the mode numbers.

In the analysis of SLGS, the effect of the nonlocal parameter $(e_0 a)$ on the vibration characteristics has been investigated. For the following analysis of DLGSs, we only focus on the discussion of the layer numbers, attached mass and vibration frequencies.

Substituting Equations (23) and (27) into Equation (26), and putting $e_0 a = 0$, yields

$$\begin{aligned} &\pi^8 \left(\frac{m^2}{L_a^2} + \frac{n^2}{L_b^2}\right)^4 Y + \frac{\left(2c - \rho h\omega^2\right)}{D} \pi^4 \left(\frac{m^2}{L_a^2} + \frac{n^2}{L_b^2}\right)^2 Y + \left[\frac{(\rho h)^2 \omega^4 - 2c\rho h\omega^2}{D^2}\right] Y \\ &= \left\{\frac{\pi^4}{D}\left(\frac{m^2}{L_a^2} + \frac{n^2}{L_b^2}\right)^2 \omega^2 - \frac{\rho h}{D^2}\omega^4 + \frac{c}{D^2}\omega^2\right\} m_c \delta(x - x_0)\delta(y - y_0) Y \end{aligned} \tag{28}$$

After multiplying both sides of Equation (28) by $\sin\frac{m\pi x}{L_a}\sin\frac{n\pi y}{L_b}$ and integrating over the whole region with respect to x and y within the limits from $x = 0$ to $x = L_a$ and $y = 0$ to $y = L_b$, after some simplifications, we obtain the following polynomial expression of the frequency

$$r_0\omega^4 - r_1\omega^2 + r_2 = 0 \tag{29}$$

where the coefficients r_0, r_1, and r_2 are

$$r_0 = \left(\frac{\rho h}{D}\right)^2 + \frac{4\rho h}{D^2 L_a L_b} m_c \sin^2 m\pi\xi \sin^2 \eta \tag{30a}$$

$$r_1 = \frac{2\rho h\pi^4}{D}\left(\frac{m^2}{L_a^2}+\frac{n^2}{L_b^2}\right)^2 + \frac{2\rho hc}{D^2} + \left[\frac{4\pi^4}{abD}\left(\frac{m^2}{L_a^2}+\frac{n^2}{L_b^2}\right)^2 + \frac{c}{D^2}\right] m_c \sin^2 m\pi\xi \sin^2 m\pi\eta \tag{30b}$$

$$r_2 = \pi^8\left(\frac{m^2}{L_a^2}+\frac{n^2}{L_b^2}\right)^4 + \frac{2c\pi^4}{D}\left(\frac{m^2}{L_a^2}+\frac{n^2}{L_b^2}\right)^2 \tag{30c}$$

where and $\xi = x_0/L_a$ and $\eta = y_0/L_b$ define the non-dimensional position of attached nanoparticles.

The solution of Equation (29) yields the resonate frequency of DLGSs. The high frequency of DLGSs with anti-phase mode, in which the upper and lower layers of DLGSs moves in the opposite direction, can be obtained from

$$\omega_{mn}^2 = \frac{r_1 + \sqrt{r_1^2 - 4r_0 r_2}}{2r_0} \tag{31}$$

3. Analytical Results and Discussion

In our simulations, the nanomechanical resonator is considered to simply consist of supported GSs loaded with a nanoparticle. The vibration mode is taken to be the fundamental frequency of $m = n = 1$, and the anti-phase mode in which the deflection of the upper and lower layers in DLGSs occurs in the opposite direction. In order to investigate the vibration behavior of a realistic graphene-based nanoscale mechanical mass sensor, the geometrical dimensions and the material constants were taken from the recent literature. The aspect ratio of the DLGSs is defined as the side length to thickness 2*h*ratio, where the effective thickness *h* of each layer is 0.127 nm. The equivalent Young's modulus *E* and density ρ of the GSs are taken to be 2.81 TPa and 2300 kg/m^3, respectively [49].

Figures 2 and 3 show the resonant frequency and the frequency shift of SLGSs as a function of the attached nanomass for different nonlocal parameters. Here, the frequency shift is defined as the difference between the natural frequency of a GS with and without attached nanoparticles, *i.e.*, $\Delta\omega = \Delta(\omega) - \Delta(\omega + m_c)$. The nanoparticles are attached on the center ($\xi = \eta = 0.5$) of the GSs with $L_a/2h = L_b/2h = 20$. The resonant frequency shown in Figure 2 decreases with increasing mass of attached nanoparticles. It is observed form Figure 3 that the frequency shift ($\Delta\omega$) of GSs carrying attached nanoparticles is positive because the attached particles increase the overall mass of the GS resonator, and the value of the shift increases with increasing attached mass. For the nonlocal parameter $e_0 a$ used in this simulation, we take that $e_0 a$ is 0, 1.0 nm and 2.0 nm [50–52]. The adopted value of the scaling parameter e_0 depends on the crystal structure in lattice dynamics, and the internal characteristics

length a = 1.42 nm (C-C bond length) for the graphene structure. The nonlocal parameter affects the vibration simulation results of the GSs due to the size-dependent mechanical properties. It is found that the influence of the nonlocal parameter on the frequency shift becomes larger when the GSs carry a relatively small mass of nanoparticles.

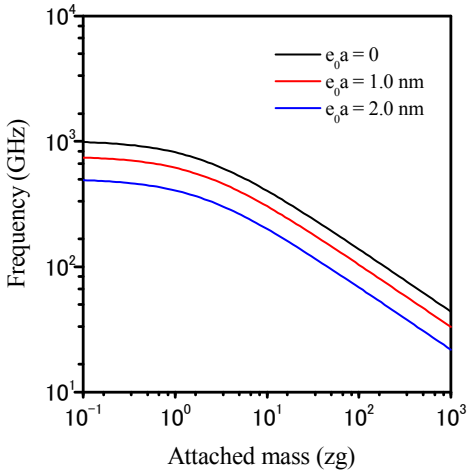

Figure 2. Variation of the resonant frequency in SLGSs as a function of attached mass for different nonlocal parameter ($L_a/2h = L_b/2h = 20, \xi = \eta = 0.5$).

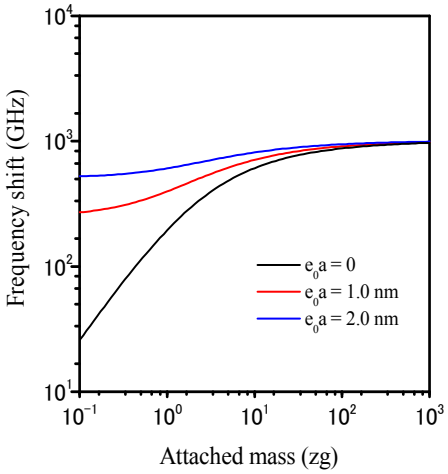

Figure 3. Variation of the frequency shift in SLGSs as a function of attached mass for different nonlocal parameter ($L_a/2h = L_b/2h = 20, \xi = \eta = 0.5$).

A comparison of the resonant frequency and the frequency shift between the SLGSs and DLGSs is shown in Figures 4 and 5 as a function of the mass of the nanoparticles attached to the center of sheet. As shown in Figure 4, the value of resonant frequency decreases with increasing mass and the DLGSs have higher vibration frequency than the SLGSs. It is seen in Figure 5 that the frequency shift of the GS resonator increases with increasing nanoparticle mass, especially for DLGSs. This suggests that DLGSs used as nanomechanical resonator can provide higher sensitivity than SLGSs. The relationship between the frequency shift and the attached mass is nearly logarithmic linear for small attached masses. The linear relationship of DLGSs has a wider range than that of SLGSs. Thus, the result indicates that DLGSs can more easily be used to estimate the attached mass than SLGSs according to the changes in the

resonant frequency. The double logarithmic linear relationship of the DLGSs is less than about 1.0 zg. According to this simulation, the relationship between the frequency shift ($\Delta\omega$) and the attached mass (m_c) can be well represented by the exponential function of $\Delta\omega = \alpha m_c^{\beta}$, which has a double logarithmic, linear relationship. The values of the parameters α and β can be determined easily by fitting the experimental results. It is seen that the variation of frequency shifts of the DLGSs agrees qualitatively with the results for circular and square SLGSs reported by Lei *et al.* [40] and Shen *et al.* [42]. The frequency shift appears when the attached mass is less than 1.0 zg, and thus the mass sensitivity of this kind of DLGS resonator can reach the range of atomic mass unit.

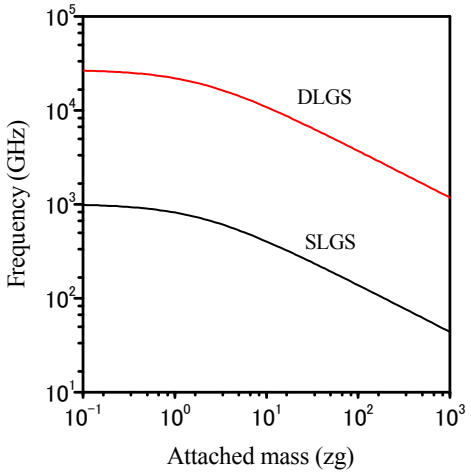

Figure 4. Comparison of the resonant frequency variation for DLGSs- and SLGSs-based mass sensors ($L_a/2h = L_b/2h = 20, \xi = \eta = 0.5$).

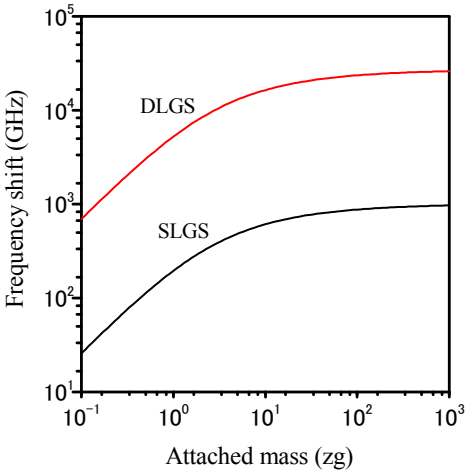

Figure 5. Comparison of the frequency shift for DLGSs- and SLGSs-based on mass sensor ($L_a/2h = L_b/2h = 20, \xi = \eta = 0.5$).

The effect of the location of attached nanoparticles on the frequency shift of the DLGSs is shown in Figure 6. The attached mass is located either at the center $(\xi, \eta) = (0.5, 0.5)$ of the DLGSs, near to the corner $(\xi, \eta) = (0.25, 0.25)$, or near to the edge $(\xi, \eta) = (0.5, 0.25)$. It can be found that the location of the nanoparticles influences the frequency shift significantly. The value of the frequency shift rises as the mass is close to the center of the DLGSs, but the dependence on location becomes smaller when the

attached mass increases. Figure 7 shows the DLGSs aspect ratio (length to width) effect on the frequency shift of DLGSs with an attached nanoparticle at the center. The DLGS dimension significantly affects the frequency shift, which becomes larger as one side length of the DLGS decreases. The double logarithmic relationship between the frequency shift and the attached mass becomes highly linear when the side length of DLGS increases.

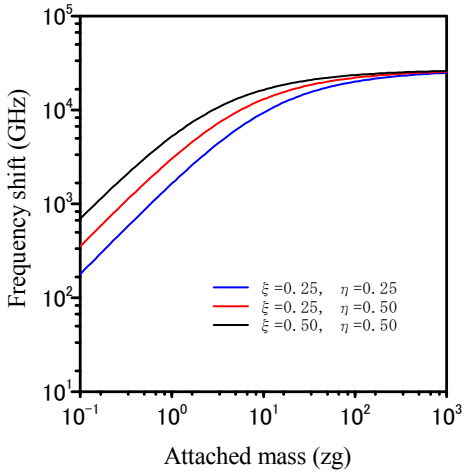

Figure 6. Location effect of the attached nanoparticle on the frequency shift of DLGS resonator ($L_a/2h = L_b/2h = 20$).

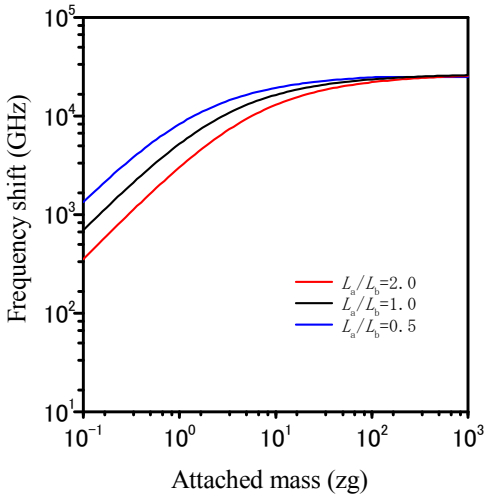

Figure 7. Influence of DLGS dimension on the frequency shift of nanomechanical resonator ($L_b/2h = 20$, $\xi = \eta = 0.5$).

Finally, Figure 8 indicates the relationship between the frequency shift and the aspect ratio of DLGSs with different attached masses. The resonant frequency is sensitive to the side length of DLGSs due to the stiffness dependence of DLGS resonators, especially for small masses of the nanoparticles. It is found that the frequency shift of the DLGS resonator increases with increasing attached mass and decreasing aspect ratio. This suggests that, to provide higher sensitivity, the dimension of the DLGSs used as sensor elements can be changed.

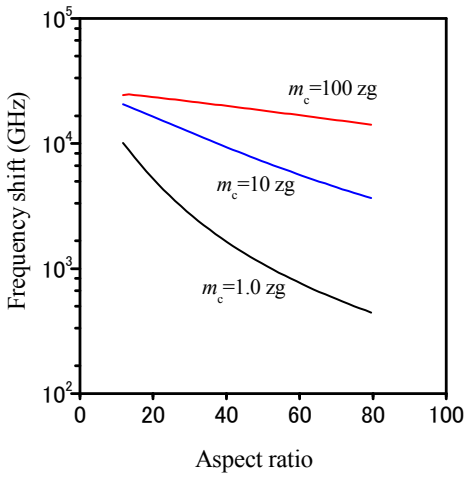

Figure 8. Relationship between the frequency shift and the aspect ratio of DLGSs for different attached mass ($\xi = \eta = 0.5$).

4. Conclusions

Based on nonlocal elasticity theory, we present a vibration analysis of supported DLGSs carrying an attached mass, taking the small-scale effect into account. The DLGSs are regarded as two single-layered GSs coupled by vdW interaction forces. The mass of nanoparticles attached to the DLGSs can be derived by measuring the frequency change of the GS resonator. According to the present analytical model, the influences of the nonlocal parameters, the attached mass, and the position of the nanoparticles on the frequency shift of GSs are analyzed and discussed in detail. A logarithmically linear relationship exists between the vibration frequency and the attached mass when the total mass is less than 1.0 zg for DLGSs. Moreover, the small-scale effects considerably influence the frequency shift of GSs, especially for small masses of attached nanoparticles. The results indicate that GS resonators could provide high sensitivity as a nanomechanical mass sensor. The analytical method developed here can serve as a useful design approach for graphene-based mass sensor.

Conflicts of Interest

The author declares no conflict of interest.

References

1. Frank, I.W.; Tanenbaum, D.M.; van der Zande, A.M.; McEuen, P.L. Mechanical properties of suspended graphene sheets. *J. Vac. Sci. Technol. B* **2007**, *25*, 2558–2561.
2. Novoselov, K.S.; Geim, A.K.; Morozov, S.V.; Jiang, D.; Zhang, Y.; Dubonos, S.V.; Grigorieva, I.V.; Firsov, A.A. Electric field effect in atomically thin carbon films. *Science* **2004**, *306*, 666–669.
3. Balandin, A.A. Thermal properties of graphene and nanostructured carbon materials. *Nat. Mater.* **2011**, *10*, 569–581.
4. Du, J.; Cheng, H.M. The fabrication, properties, and uses of graphene/polymer composites. *Macromol. Chem. Phys.* **2012**, *213*, 1060–1077.

5. Chen, C.; Rosenblatt, S.; Bolotin, K.I.; Kalb, W.; Kim, P.; Kymissis, I.; Stormer, H.L.; Heinz, T.F.; Hone, J. Performance of monolayer graphene nanomechanical resonators with electrical readout. *Nat. Nanotechnol.* **2009**, *4*, 861–867.
6. Wang, X.; Zhi, L.; Mullen, K. Transparent, conductive graphene electrodes for dye-sensitized solar cells. *Nano Lett.* **2008**, *8*, 323–327.
7. Schedin, F.; Geim, A.K.; Morozov, S.V.; Hill, E.W.; Blake, P.; Katsnelson, M.I.; Novoselov, K.S. Detection of individual gas molecules adsorbed on grapheme. *Nat. Mater.* **2007**, *6*, 652–655.
8. Arash, B.; Jiang, J.W.; Rabczuk, T. A review on nanomechanical resonators and their applications in sensors and molecular transportation. *Appl. Phys. Rev.* **2015**, *2*, 021301, doi:10.1063/1.4916728.
9. Jiang, J.W.; Park, H.; Rabczuk, T. MoS2 Nanoresonators: Intrinsically better than graphene? *Nanoscale* **2014**, *6*, 3618–3625.
10. Jiang, J.W.; Wang, B.S.; Park, H.; Rabczuk, T. Adsorbate migration effects on continuous and discontinuous temperature-dependent transitions in the quality factors of graphene nanoresonators. *Nanotechnology* **2014**, *25*, 025501, doi: 10.1088/0957-4484/25/2/025501.
11. Jiang, J.W.; Park, H.; Rabczuk, T. Preserving the Q-factors of ZnO nanoresonators via polar surface reconstruction. *Nanotechnology* **2013**, *24*, 405705, doi:10.1088/0957-4484/24/40/405705.
12. Jiang, J.W.; Park, H.S.; Rabczuk, T. Enhancing the mass sensitivity of graphene nanoresonators via nonlinear oscillations: The elective strain mechanism. *Nanotechnology* **2012**, *23*, 47550, doi: 10.1088/0957-4484/23/47/475501.
13. Wang, Q.; Arash, B. A review on applications of carbon nanotubes and graphenes as nano-resonator sensors. *Comput. Mater. Sci.* **2014**, *82*, 350–360.
14. Arash, B.; Wang, Q. Detection of gas atoms with carbon nanotubes. *Sci. Rep.* **2013**, *3*, doi:10.1038/srep01782.
15. Ekinci, K.L.; Huang, X.M.H.; Roukes, M.L. Ultrasensitive nanoelectromechanical mass detection. *Appl. Phys. Lett.* **2004**, *84*, 4469–4471.
16. Chaste, J.; Eichler, A.; Moser, J.; Ceballos, G.; Rurali, R.; Bachtold, A. A nanomechanical mass sensor with yoctogram resolution. *Nat. Nanotechnol*. **2012**, *7*, 301–304.
17. Eichler, A.; Moser, J.; Chaste, J.; Zdrojek, M.; Wilson-Rae, I.; Bachtold, A. Nonlinear damping in mechanical resonators made from carbon nanotubes and graphene. *Nat. Nanotechnol.* **2011**, *6*, 339–342.
18. Pang, W.; Yan, L.; Zhang, H.; Yu, H.Y.; Kim, E.S.; Tang, W.C. Femtogram mass sensing platform based on lateral extensional mode piezoelectric resonator. *Appl. Phys. Lett.* **2006**, *88*, 243503, doi:10.1063/1.2213975.
19. Geim, A.K. Graphene: status and prospects. *Science* **2009**, *324*, 1530–1534.
20. Bunch, J.S.; van der Zande, A.M.; Verbridge, S.S.; Frank, I.W.; Tanenbaum, D.M.; Parpia, J.M.; Craighead, H.G.; McEuen, P.L. Electromechanical Resonators from Graphene Sheets. *Science* **2007**, *315*, 490–493.
21. Xu, M.S.; Gao, Y.; Yang, X.; Chen, H.Z. Unique synthesis of graphene-based materials for clean energy and biological sensing applications. *Chin. Sci. Bull.* **2012**, *57*, 3000–3009.
22. Novoselov, K.S.; Jiang, D.; Schedin, F.; Booth, T.J.; Khotkevich, V.V.; Morozov, S.V.; Geim, A.K. Two-dimensional atomic crystals. *Proc. Natl. Acad. Sci. USA* **2005**, *102*, 10451–10453.

23. Wei, D.C.; Liu, Y.Q. Controllable synthesis of graphene and its applications. *Adv. Mater.* **2010**, *22*, 3225–3241.
24. Kim, K.S; Zhao, Y; Jang, H.; Lee, S.Y.; Kim, J.M.; Kim, K.S.; Ahn, J.H.; Kim, P.; Choi, J.Y.; Hong, B.H. Large-scale pattern growth of graphene films for stretchable transparent electrodes. *Nature* **2009**, *457*, 706–710.
25. Sutter, P.W.; Flege, J.I.; Sutter, E.A. Epitaxial graphene on ruthenium. *Nat. Mater.* **2008**, *7*, 406–411.
26. Arghavan, S.; Singh, A.V. Effects of van der Waals interactions on the nonlinear vibration of multi-layered graphene sheets. *J. Phys. D: Appl. Phys.* **2012**, *45*, 455305, doi: 10.1088/0022-3727/45/45/455305
27. Ohta, T.; Bostwick, A.; Seyller, T.; Horn, K.; Rotenberg, E. Controlling the electronic structure of bilayer grapheme. *Science* **2006**, *313*, 951–954.
28. Virojanadara, C.; Yakimova, R.; Zakharov, A.A.; Johansson, L.I. Large homogeneous mono-/bi-layer graphene on 6h-sic(0001) and buffer layer elimination. *J. Phys. D Appl. Phys.* **2010**, *43*, 374010, doi: 10.1088/0022-3727/43/37/374010.
29. Zhang, Y.; Tang, T.T.; Girit, C.; Hao, Z.; Martin, M.C.; Zettl, A.; Crommie, M.F.; Shen, Y.R.; Wang, F. Direct observation of a widely tunable bandgap in bilayer grapheme. *Nature* **2009**, *459*, 820–823.
30. Meng, H.; Dai, Y.; Ye, Y.; Luo, J.X.; Shi, Z.J.; Dai, L.; Qin, G.G. Bilayer graphene anode for small molecular organic electroluminescence. *J. Phys. D Appl. Phys.* **2012**, *45*, 245103, doi: 10.1088/0022-3727/45/24/245103.
31. Popov, A.M.; Lebedeva, I.V.; Knizhnik, A.A.; Lozovik, Y.E.; Potapkin, B.V. Structure, energetic and tribological properties, and possible applications in nems of argon-separated double-layer grapheme. *J. Phys. Chem. C* **2013**, *117*, 11428–11435.
32. Popov, A.M.; Lebedeva, I.V.; Knizhnik, A.A.; Lozovik, Y.E.; Potapkin, B.V.; Poklonski, N.A.; Siahlo, A.I.; Vyrko, S.A. AA stacking, tribological and electronic properties of double-layer graphene with krypton spacer. *J. Chem. Phys.* **2013**, *139*, 154705, doi:10.1063/1.4824298.
33. Wang, J.; He, X.; Kitipornchai, S.; Zhang, H. Geometrical nonlinear free vibration of multi-layered graphene sheets. *J. Phys. D Appl. Phys.* **2011**, *44*, 135401, doi: 10.1088/0022-3727/44/13/135401.
34. Shi, J.X.; Ni, Q.Q.; Lei, X.W.; Natsuki, T. Nonlocal vibration of embedded double-layer graphene nanoribbons in in-phase and anti-phase modes. *Phys. E* **2012**, *44*, 1136–1141.
35. Natsuki, T.; Shi, J.X.; Ni, Q.Q. Vibration analysis of circular double-layered graphene sheets. *J. Appl. Phys.* **2012**, *111*, 044310, doi: 10.1142/S1758825112500391.
36. Hill, E.W.; Vijayaraghavan, A.; Novoselov, K. Graphene sensors. *IEEE Sens. J.* **2011**, *11*, 3161–3170.
37. Arash, B.; Wang, Q.; Duan, W.H. Detection of gas atoms via vibration of graphenes. *Phys. Lett. A* **2011**, *375*, 2411–2415.
38. Jiang, J.W.; Park, H.S.; Rabczuk, T. Enhancing the mass sensitivity of graphene nanoresonators via nonlinear oscillations: The effective strain mechanism. *Nanotechnology* **2012**, *23*, 475501, doi: 10.1088/0957-4484/23/47/475501.
39. Sakhaee-Pour, A.; Ahmadiana, M.T.; Vafaib, A. Applications of single-layered graphene sheets as mass sensors and atomistic dust detectors. *Solid State Commun.* **2008**, *145*, 168–172.

40. Lei, X.W.; Natsuki, T.; Shi, J.X.; Ni, Q.Q. Vibration analysis of circular double-layered graphene sheets. *J. Appl. Phys.* **2013**, *113*, 154313, doi: 10.1063/1.3686689.
41. Dai, M.D.; Kim, C.W.; Eom, K. Nonlinear vibration behavior of graphene resonators and their applications in sensitive mass detection. *Nanoscale Res. Lett.* **2012**, *7*, 449, doi:10.1186/1556-276X-7-499.
42. Shen, Z.B.; Tang, H.L.; Li, D.K.; Tang, G.J. Vibration of single-layered graphene sheet-based nanomechanical sensor via nonlocal kirchhoff plate theory. *Comp. Mater. Sci.* **2012**, *61*, 200–205.
43. Lee, H.L.; Yang, Y.C.; Chang, W.J. Mass Detection Using a Graphene-Based Nanomechanical Resonator. *Jpn. J. Appl. Phys.* **2013**, *52*, 025101, doi: 10.7567/JJAP.52.025101.
44. Natsuki, T.; Shi, J.X.; Ni, Q.-Q. Vibration analysis of nanomechanical mass sensor using double-layered graphene sheets resonators. *J. Appl. Phys.* **2013**, *114*, 094307, doi:10.1063/1.4820522.
45. Lu, P.; Zhang, P.Q.; Lee, H.P.; Wang, C.M.; Reddy, J.N. Non-local elastic plate theories. *Proc. R. Soc. A* **2007**, *463*, 3225–3240.
46. Polizzotto, C. Nonlocal elasticity and related variational principles. *Inter. J. Solid. Struc.* **2001**, *38*, 7359–7380.
47. Arash, B.; Wang, Q. A review on the application of nonlocal elastic models in modeling of carbon nanotubes and graphenes. *Comput. Mater. Sci.* **2012**, *51*, 303–313.
48. Kitipornchai, S.; He, X.Q.; Liew, K.M. Continuum model for the vibration of multilayered graphene sheets. *Phys. Rev. B* **2005**, *72*, 075443, doi:10.1103/PhysRevB.72.075443.
49. Shi, J.X.; Natsuki, T.; Lei, X.W.; Ni, Q.Q. Equivalent Young's modulus and thickness of graphene sheets for the continuum mechanical models. *Appl. Phys. Lett.* **2014**, *104*, 223101, doi:10.1063/1.4880729.
50. Narendar, S.; Gopalakrishnan, S. Nonlocal scale effects on wave propagation in multi-walled carbon nanotubes. *Comput. Mater. Sci.* **2009**, *47*, 526–538.
51. Amiriana, B.; Hosseini-Arab, R.; Moosavia, H. Thermo-mechanical vibration of short carbon nanotubes embedded in pasternak foundation based on nonlocal elasticity theory. *Shock. Vib.* **2013**, *20*, 821–832.
52. Duan, W.H.; Wang, C.M.; Zhang, Y.Y. Calibration of nonlocal scaling effect parameter for free vibration of carbon nanotubes by molecular dynamics. *J. Appl. Phys.* **2007**, *101*, 024305, doi:10.1063/1.2423140.